Technology in Cancer Research and Treatment
ISSN 1533-0346
Volume 11, Number 4, August 2012

Comparison of BOLD Cerebrovascular Reactivity Mapping and DSC MR Perfusion Imaging for Prediction of Neurovascular Uncoupling Potential in Brain Tumors

www.tcrt.org

Jay J. Pillai, M.D.[1]*
Domenico Zacà, Ph.D.[1]*

[1]Neuroradiology Division, Russell H. Morgan Department of Radiology and Radiological Science, The Johns Hopkins University School of Medicine & The Johns Hopkins Hospital, 600 N. Wolfe Street, Phipps B-100, Baltimore, MD, USA
*Both authors contributed equally

The coupling mechanism between neuronal firing and cerebrovascular dilatation can be significantly compromised in cerebral diseases, making it difficult to identify eloquent cortical areas near or within resectable lesions by using Blood Oxygen Level Dependent (BOLD) fMRI. Several metabolic and vascular factors have been considered to account for this lesion-induced neurovascular uncoupling (NVU), but no imaging gold standard exists currently for the detection of NVU. However, it is critical in clinical fMRI studies to evaluate the risk of NVU because the presence of NVU may result in false negative activation that may result in inadvertent resection of eloquent cortex, resulting in permanent postoperative neurologic deficits. Although NVU results from a disruption of one or more components of a complex cellular and chemical neurovascular coupling cascade (NCC) MR imaging is only able to evaluate the final step in this NCC involving the ultimate cerebrovascular response. Since anything that impairs cerebrovascular reactivity (CVR) will necessarily result in NVU, regardless of its effect more proximally along the NCC, we can consider mapping of CVR as a surrogate marker of NVU potential. We hypothesized that BOLD breath-hold (BH) CVR mapping can serve as a better marker of NVU potential than T2* Dynamic Susceptibility Contrast gadolinium perfusion MR imaging, because the latter is known to only reflect NVU risk associated with high grade gliomas by determining elevated relative cerebral blood volume (rCBV) and relative cerebral blood flow (rCBF) related to tumor angiogenesis. However, since low and intermediate grade gliomas are not associated with such tumoral hyperperfusion, BOLD BH CVR mapping may be able to detect such NVU potential even in lower grade gliomas without angiogenesis, which is the hallmark of glioblastomas. However, it is also known that glioblastomas are associated with variable NVU, since angiogenesis may not always result in NVU. Perfusion metrics obtained by T2* gadolinium perfusion MR imaging were compared to BOLD percentage signal change on BH CVR maps in a group of 19 patients with intracranial brain tumors of different nature and grade. Single pixel maximum rCBV and rCBF within holotumoral regions of interest (*i.e.*, "ipsilesional" ROIs) were normalized to contralateral hemispheric homologous (*i.e.*, "contralesional") normal tissue. Furthermore, percentage signal change on BH CVR maps within ipsilesional ROIs were normalized to the percentage signal change within contralesional homologous ROIs. Inverse linear correlation was found between normalized rCBF (r_{flow}) or rCBV (r_{vol}) and normalized CVR percentage signal change (r_{CVR}) in grade IV lesions. In the grade III lesions a less steep inverse linear trend was seen that did not reach statistical

Abbreviations: BOLD fMRI: Blood Oxygen Level Dependent Functional Magnetic Resonance Imaging; NVU: Neurovascular Uncoupling; T2* DSC: T2* Dynamic Susceptibility Contrast; CVR: CerebroVascular Reactivity; BH: Breath Hold; rCBV: Relative Cerebral Blood Volume; rCBF: Relative Cerebral Blood Flow; MTT: Mean Transit Times; PSC: Percentage Signal Change; NCC: Neurovascular Coupling Cascade.

*Corresponding author:
Jay J. Pillai, M.D.
E-mail: jpillai1@jhmi.edu

significance, whereas no correlation at all was seen in the grade II group. Statistically significant difference was present for r_{flow} and r_{vol} between the grade II and IV groups and between the grade III and IV groups but not for r_{CVR}. The r_{CVR} was significantly lower than 1 in every group. Our results demonstrate that while T2*MR perfusion maps and CVR maps are both adequate to map tumoral regions at risk of NVU in high grade gliomas, CVR maps can detect areas of decreased CVR also in low and intermediate grade gliomas where NVU may be caused by factors other than tumor neovascularity alone. Comparison of areas of abnormally decreased regional CVR with areas of absent BOLD task-based activation in expected eloquent cortical regions infiltrated by or adjacent to the tumors revealed overall 95% concordance, thus confirming the capability of BH CVR mapping to effectively demonstrate areas of NVU.

Key words: BOLD fMRI; Presurgical Mapping; CerebroVascular Reactivity; Neurovascular Uncoupling.

Introduction

The coupling mechanism between neuronal firing and cerebrovascular dilatation can be significantly compromised in cerebral diseases, making it difficult to identify eloquent cortical areas near or within resectable lesions by using Blood Oxygen Level Dependent (BOLD) fMRI (1). Several metabolic and vascular factors have been considered to account for this lesion-induced neurovascular uncoupling (NVU), but no imaging gold standard exists currently for the detection of NVU (2). However, it is critical in clinical BOLD fMRI studies to evaluate the risk of NVU because the presence of NVU may result in false negative activation. Such false negative activation in presurgical BOLD fMRI may lead to catastrophic resection of apparently "silent" eloquent cortex, which is incapable of producing a BOLD response, if intraoperative electrophysiological confirmation is not performed. However, NVU may involve disruption of any of a number of components comprising a complex cascade from activated neurons to neurotransmitters to astrocytes to chemical mediators and finally vascular smooth muscle (17). For purposes of this paper, we will refer to this as the neurovascular coupling cascade. While it is impossible to detect NVU at the neuronal, astrocytic, neurotransmitter or chemical mediator levels by MR imaging alone, it is possible to evaluate the final step in this cascade: the cerebrovascular response. Since anything that impairs cerebrovascular reactivity (CVR) will necessarily result in NVU, regardless of its effect more proximally along the cascade, we can consider mapping of CVR as a surrogate marker of NVU potential. T2* Dynamic Susceptibility Contrast (DSC) gadolinium perfusion MR imaging seems to indirectly evaluate NVU risk in high grade gliomas (4), where elevated relative cerebral blood volume (rCBV) and relative cerebral blood flow (rCBF) have been associated with tumor neovascularity, which in turn is associated with impaired CVR that is responsible for NVU. However, it is not clear how high the prevalence of impaired CVR (and resultant NVU) is in low grade gliomas, in which hyperperfusion is unusual. The goal of this study is to demonstrate that BOLD CVR mapping using a breath hold (BH) paradigm is a feasible method of evaluating CVR in all tumor grades, including in low and intermediate grade gliomas that are not typically associated with regional hyperperfusion, and as such, BOLD BH CVR mapping may serve as a superior marker of NVU potential than MR perfusion imaging. This imaging marker would be independent of the activation task or neural stimulus that may be applied in clinical fMRI examinations. In addition, BH CVR allows dynamic evaluation of CVR, whereas T2*DSC perfusion MRI only allows for resting state evaluation of perfusion. Nevertheless, in spite of its limitations, T2*DSC MR perfusion imaging is the only currently available alternative approach that can be readily used in the clinical MR imaging setting to assess tumor vascularity. In this study, we compared BH CVR mapping results and T2*DSC perfusion metrics in a population of grade II (low grade), III (anaplastic) and IV (glioblastoma) primary intra-axial brain tumors (gliomas), to assess the relative value of these two techniques as imaging markers of NVU potential.

Materials and Methods

Participants

Nineteen patients with histopathologically proved brain tumors were included in this retrospective study that was approved by our Institutional Review Board and was compliant with the Health Insurance Portability and Accountability Act. Tumor classification was determined according to the guidelines provided by the World Health Organization (WHO) (5). Table I reports demographic data including age, tumor location and histology for each patient included in the study.

Image Acquisition

Studies were performed on a Siemens 3T Trio system (Siemens Medical Solution, Erlangen, Germany) equipped with a head matrix coil.

BOLD images were acquired by a whole brain single-shot T2*-weighted Gradient-Echo EPI sequence with the following parameters: TR = 2000 ms; TE = 30 ms; 90° flip angle; 24 cm field of view; 64 × 64 matrix acquisition; slice thickness 4 mm with 1 mm gap between slices. Each patient recruited in the study performed a battery of block design language and motor tasks, 3 or 4 minutes long. The actual language, motor and visual tasks are listed in Table I. The actual number and type of paradigms varied from patient

to patient depending on the location of the lesion and the patients neurological conditions. In addition they performed also a BH task that included four cycles of alternating normal breathing and BH periods. Each normal breathing period of 40 seconds duration was followed by a 4 second block of inspiration that immediately preceded a 16-second BH period. At the end of the last BH period an additional normal breathing period of 20 seconds was added. This was done in order to measure more accurately the hemodynamic response function due to the BH task. A 10-15 sec delay between the task and the expected hemodynamic response function has indeed been demonstrated in a recent work by Birn and others (6).

Visual or auditory cues were used during the paradigms, that were commercially available or implemented in Prism Acquire Software (Prism Clinical Imaging, Elm Grove, WI, USA).

Patients were monitored via a LCD monitor outside the scanner room to assess tasks performance. A training session was performed outside the scanner in order to familiarize the patients with the tasks and to assess whether they were able to properly follow the instructions, particularly to hold their breath for the required amount of time. They were also instructed to keep their head absolutely still without motion throughout the entire study. However, head motion was minimized by using straps and foam paddings. All the patients were able to successfully perform the tasks.

Dynamic Susceptibility Contrast perfusion MRI was carried out within the same examination session after BOLD fMRI images were acquired. A whole brain single-shot T2*-weighted Gradient-Echo EPI sequence was used for perfusion imaging to measure signal change due to intravenous bolus injection of a Gadolinium-based contrast agent (Magnevist, concentration 0.1 mmol/kg). Imaging parameters were the following: TR = 2450 ms; TE = 45 ms; 90° flip angle; 24 cm field of view; 128 × 128 matrix acquisition; slice thickness 4 mm with 1 mm interslice gap. 32 volumes were acquired and the first two were discarded to allow the MR signal to reach steady state.

Pre and post contrast 3D T1-weighted Magnetization Prepared Rapid Acquisition Gradient Echo (MPRAGE) images were acquired. Imaging parameters were: TR = 7 ms; TE = 3.5 ms; 9° flip angle; 24 cm field of view; 256 × 256 matrix acquisition; slice thickness 1 mm. A susceptibility weighted imaging (SWI) sequence was also carried out with the following parameters: TR = 27 ms, TE = 20 ms, 15° flip angle, 24 cm field of view, 256 × 256 matrix acquisition, slice thickness 1.5 mm.

Image Processing

The imaging datasets acquired for every patient were transferred to an external workstation and pre-processing was performed using DynaSuiteNeuro software (InVivo Corporation, Pewaukee, WI, USA).

The T1 post contrast images and the SWI were coregistered with the T1 pre contrast images by using a rigid body algorithm.

The raw BOLD EPI BH task data were first temporally interpolated to correct the fact that different slices were acquired at different times, and then each volume was registered to a reference one to correct for mild head motion during the acquisition of functional data. This time-shifted and motion-corrected dataset was then coregistered with the T1 pre contrast images by a rigid body algorithm.

Raw perfusion images were motion-corrected and then coregistered with T1 pre contrast images by a rigid body algorithm. Signal-time curves were then converted into concentration-time curves assuming an inverse proportionality relationship between these two quantities. The rCBV was calculated integrating the concentration-time curve and adding a correction factor to take into account the contrast leakage through the disrupted blood-brain barrier, computed according to the method developed by Boxerman *et al*. (7). MTT was calculated as first moment of the first pass curve. Then rCBF was derived, according to the central volume principle, from the ratio:

$$\mathrm{rCBF} = \frac{\mathrm{rCBV}}{\mathrm{MTT}} \qquad [1]$$

The regression analysis for generation of BOLD cerebrovascular reactivity (CVR) maps was then carried out using Analysis of Functional NeuroImages (AFNI) software. Datasets were first spatially smoothed with a 4 mm Gaussian Kernel. General Linear Model (GLM) analysis was performed where the acquired BOLD signal time series was fitted voxel by voxel to the following function:

$$y(t) = \beta_0 + \beta_1 t + \alpha x(t) \qquad [2]$$

where β_0 and β_1 are the coefficients of a first grade polynomial that models the baseline as a constant (β_0) plus a linear temporal trend (β_1), $x(t)$ is the ideal hemodynamic times series (ideal T.S.) obtained convolving a special hemodynamic impulse response function for a respiratory task with the BH paradigm timing, and α its coefficient (6). A voxel by voxel map of the regressors α, β_0 and β_1 was calculated as a result of the fit.

Table I

Demographic information, including age, sex, lobar tumor location and pathology (columns 1-4), assessment of concordance between regional decreased CVR and absence of expected eloquent cortical activation (column 5), listing of fMRI task types, *i.e.*, motor, language or visual (column 6), anatomic gyral location of absent BOLD activation and corresponding regional decreased CVR (column 7), specific fMRI tasks performed (column 8) and exact anatomic location of "BOLD-silent" eloquent cortex with respect to tumor margins (final column 9) for nineteen brain tumor cases included in this study.

Age	Sex	Tumor location	Pathology (WHO grade and histology)	Concordance between regionally decreased CVR and absence of expected activation — Yes (Y) or No (N)	Tasks for which absent expected activation was noted corresponding to areas of regionally decreased CVR—motor (M), language (L), or visual (V)	Gyrus in which expected activation was absent in regions of decreased CVR	Specific paradigms which demonstrated absent activation in expected eloquent cortex demonstrating regionally decreased CVR	Exact anatomic location of "BOLD-silent" eloquent cortex with respect to tumor margins
78	F	Left frontal	Glioblastoma Grade IV	Y	L	LIFG	SC, LC, Rhym	Posterior to lesion
29	M	Left frontal	Anaplastic astrocytoma grade III	Y	M	L precentral gyrus	FingM, LipM	Lateral and superomedial to lesion
34	M	Left temporal	Glioblastoma multi-forme grade IV	Y	L	LSTG, LMTG	SC, SWG, Rhym	Lateral to lesion
28	M	Left temporal	Astrocytoma grade II	Y	L	LSTG, LMTG	SWG, SC, Rhym, LC, PL	Lateral to lesion
42	M	Right frontotemporal	Glioblastoma multi-forme grade IV	Y	L	RIFG, RMTG	SC, Rhym, LC, PL	Lateral, anterolateral to lesion
60	F	Right parietal	Oligodendroglioma grade II	Y	M	R postcentral gyrus	ToeM, AnkleM	Anterior to & including lesion
54	M	Left occipital	Glioblastoma Grade IV	Y	V	Occipital cortex along L calcarine sulcus	Vwedge, Vring	Posteromedial to lesion
40	M	Right frontoparietal	Glioblastoma multi-forme grade IV	Y	M, L	R precentral gyrus (motor), R SFG (language–preSMA)	SWG, SC, Rhym (language), FootM, FingM (motor)	Medial (preSMA, foot PMC), posterolateral (hand PMC)
60	M	Left temporal	Glioblastoma Grade IV	Y	L	L STG	SC, Rhym, LC	Lateral to lesion
54	M	Left frontal	Oligodendroglioma grade II	Y	M, L	L SFG (SMA & preSMA), Foot & face RA of L PMC (precentral gyrus)	TM, ToeM, FootM–motor; SWG, SC, Rhym–language	Superomedial to lesion (SMA) & posterolateral to lesion (face RA of PMC) & posteromedial to lesion (foot RA of PMC)

45	F	Right temporoparietal	Anaplastic Oligodendroglioma grade III	Y	M	R precentral gyrus (hand RA)	HandM-R&L	Along anterior and lateral aspects of mass–within lesion
42	M	Left temporal	Astrocytoma grade II	Y	L	LSTG, LMTG	SWG, Rhym, LC, PL	Along lateral aspect of mass–within and adjacent to tumor
27	M	Right posterior cingulate And medial frontoparietal	Oligodendroglioma grade II	Y	M	RSFG (SMA, Foot RA PMC)	ToeM, FootM	Superior and superomedial to lesion
25	F	Left medial frontal	Oligoastrocytoma grade II	Y	L, M	L SFG (motor and language SMA)	FingM, HandM, FootM, SWG, SC, Rhym, LC	Medial aspect of mass
46	M	Left frontoparietal	Glioblastoma multiforme grade IV	Y	M	L precentral gyrus	HandM, TM	Lateral aspect of mass
29	M	Right parietal	Anaplastic Astrocytoma grade III	Y	M	R postcentral gyrus	HandM, FingM, FootM	Anterolateral tumor margin—within tumor
69	F	Right parietal	Anaplastic Oligodendroglioma grade III	Y	M	R postcentral gyrus	TM, FingM	Anterior margin of tumor
34	F	Right perirolandic	Anaplastic Astrocytoma grade III	Y	M	R postcentral gyrus	HandM, TM, FootM	Anterior margin of tumor–within lesion
41	M	Left insula & basal ganglia	Oligoastrocytoma grade II	N	L	None; no eloquent cortex involved by tumor–insula and basal ganglia involved only	SWG, SC, Rhym, LC	BA, WA and LMTG all activated and not affected by tumor

The legend for abbreviations in the table is as follows:

M—Male; F—Female; L—Left; R—Right; IFG—Inferior frontal gyrus; STG—Superior temporal gyrus; MTG—Middle temporal gyrus; SFG—Superior frontal gyrus; PMC—Primary motor cortex; RA—Representation area; SMA—Supplementary motor area; SC—Sentence completion task; LC—Sentence listening comprehension task; SWG—Silent word generation task; Rhym—Rhyming task; PL—Passive story listening task; FingM—Bilateral sequential finger tapping task; HandM—Unilateral alternating hand opening/closing task; TM—Tongue motor task; ToeM—Toe flexion/extension task; FootM—Ankle flexion/extension task; LipM—Lip puckering movement task; BA—Broca's area; WA—Wernicke's area; Vwedge—Vision activation task utilizing rotating checkerboard wedge stimuli; Vring—Vision activation task utilizing expanding and contracting checkerboard ring stimuli.

CVR maps were expressed as BOLD percentage signal change (PSC) from the baseline according to the following equation:

$$\mathrm{PSC} = 100 \cdot \frac{a \cdot \mathrm{PP(ideal\ T.S.)}}{\mathrm{Baseline}} \quad [3]$$

where

PP: Peak to Peak

and

PP (ideal T.S.) = max (ideal T.S.) − min (ideal T.S.)

and

$$\mathrm{Baseline} = \beta_0 + \beta_1 \cdot (\text{average polynomial grade 1}) + a \cdot \min(\text{ideal T.S.})$$

SWI images were visually inspected to assess the presence of large susceptibility artifacts due to excessive quantities of blood products or calcification/micromineralization that could affect the subsequent Region of Interest Analysis (ROI) for BOLD CVR percentage signal change, rCBV and rCBF.

T1 post contrast images, CVR BOLD percentage signal change and rCBV and rCBF maps were imported into MIPAV (mipav.cit.nih.gov) [Medical Image Processing, Analysis and Visualization] software for ROI analysis. For each patient two observers (JJP, a subspecialty board-certified neuroradiologist with more than 13 years of experience with functional MR neuroimaging and DZ, an imaging scientist with more than 5 years of experience with physiologic MR neuroimaging as well as a PhD in functional MR imaging), who served as independent raters, selected imaging ROIs. These ROIs (referred to in the manuscript as "ipsilesional") encompassed the entire gadolinium-enhancing areas, including internal necrotic components, in the lesions showing enhancement, whereas they included the areas of hypointensity on the T1 post contrast images in the non enhancing lesions. However, large venous structures were excluded from the ROIs in order to avoid large venous effects on the metrics derived from BOLD signal (CVR) and to avoid spuriously increased perfusion measurements.

Contralateral to the tumor (*i.e.,* contralesional) homologous ROIs were drawn also. See the first figure (Figure 1) for an example of placed ROIs in three cases. Note that the ROIs encompassed the entirety of the tumors and also included cortex infiltrated by the tumor and/or immediately adjacent perilesional cortex. The ratio (r_{vol}) between the maximum rCBV value in the ipsilesional ROI and the mean rCBV value in the contralesional ROI was calculated. An identical metric was also reported for rCBF (r_{flow}). For CVR maps the ratio between the mean BOLD percentage signal change in the ipsilesional ROI and the mean BOLD percentage signal change in the contralesional ROI was calculated (r_{CVR}).

Finally, a visual inspection was performed by consensus between the two raters (JJP, DZ) of postprocessed composite motor and/or language BOLD task-related activation maps available on our institutional PACS server as part of each patient's electronic medical record. Determination was made in each case of whether regions of absent expected eloquent cortical activation on the task-related BOLD activation maps corresponded to areas of regionally decreased CVR on the BOLD BH CVR maps; this was considered the standard for the establishment of NVU in each of the 19 cases in our cohort. Such concordance or discordance was recorded for each patient (Table I).

Statistical Methods

Intraclass correlation coefficients (ICCs), *i.e.* the ratio of the between subject variance to the total variance of measurements, was calculated for r_{vol}, r_{flow} and r_{CVR}. The mean value and the standard deviation were reported for these measurements. Statistical correlation analysis between r_{vol} and r_{CVR} and between r_{flow} and r_{CVR} was performed, using the mean values, by simple regression separately for each tumor grade. Non parametric Kruskall Wallis and Mann Whitney statistical tests were performed to investigate the difference between r_{vol}, r_{flow} and r_{CVR} distributions among the different tumor grades. A one sample Wilcoxon test was performed also to assess in which patient population the CVR normalized ratio was significantly lower than 1. Statistical Analysis was performed using OriginPro 8.0.

Results

No cases were considered to be affected by severe susceptibility artifacts such that they needed to be excluded from the ROI analysis. In all cases in this study, there was nearly 100% concordance between areas of absent expected activation in eloquent sensorimotor and/or language areas on task-related BOLD activation maps, as visualized on our postprocessed clinical fMRI images available on our PACS server as part of each patient's electronic medical record, and areas of regionally decreased CVR on the BOLD BH CVR maps. This confirmed that the regionally decreased CVR in each patient reflected a high risk of NVU. As Table I shows, overall 94.7% concordance (18/19) was seen, with only one outlier, which represented a deeply seated tumor involving only left insular cortex and left basal ganglia without any extension to left frontal or temporal cortex in areas of expected eloquent language cortical activation (*e.g.*, Broca's area [left inferior frontal gyrus], Wernicke's area [left superior temporal gyrus], middle

or inferior temporal gyri). In Figure 2 two examples are shown displaying composite task-based BOLD activation maps and corresponding BH CVR maps for a grade II and a grade IV case included in this study. In both cases there is absence of task-related activation in areas of regionally decreased CVR; in case I, absence of expected Wernicke's area activation is seen on receptive language tasks despite left language dominance in this right handed patient, while in case II, on a sensorimotor task in which bilateral symmetric activation is expected, absence of activation is seen ipsilesionally in the right primary somatosensory cortex despite presence of clinically partially preserved left hand motor and sensory function.

In Table II, the r_{CVR}, r_{vol}, and r_{flow} are reported for each patient as computed by the two raters together with the average values and associated standard deviations. The ICC value for each of three considered variables is also reported that showed excellent inter-rater reliability for r_{CVR} (ICC = 0.97) as well as for r_{vol} and r_{flow} (ICC = 0.94 and ICC = 0.95, respectively) values.

In the grade IV tumor group, a statistically significant linear inverse correlation was found between r_{CVR} and r_{flow} ($r = -1.46$, $p = 0.03$), and a trend level linear inverse correlation was found between r_{CVR} and r_{vol} (slope $r = -1.20$, $p = 0.08$) (see Figure 3). In the grade III group a linear inverse relationship was seen, although less robust than with the grade IV group, and no statistically significant correlation was seen between either r_{vol} or r_{flow} and r_{CVR} ($r = -0.85$, $p = 0.46$ for r_{vol} and $r = -0.72$, $p = 0.59$ r_{flow}). In the grade II group mild but insignificant positive linear relationships were noted between r_{CVR} and r_{vol}, as well as between r_{CVR} and r_{flow} ($r = 0.40$, $p = 0.50$ for r_{vol} and $r = 0.38$, $p = 0.52$ for r_{flow}).

r_{vol} and r_{flow} distributions were significantly different among the three groups according to the results of the Kruskal Wallis test (H = 9.71, $p = 0.008$ for r_{vol} and H = 12.93, $p = 0.001$ for r_{flow}). Multiple comparison Mann Whitney non parametric tests reported statistically significant differences in the distributions of r_{vol} and r_{flow} between grade II and IV ($z = -2.44$, $p = 0.007$ and $z = -3.07$, $p = 0.001$, respectively) and

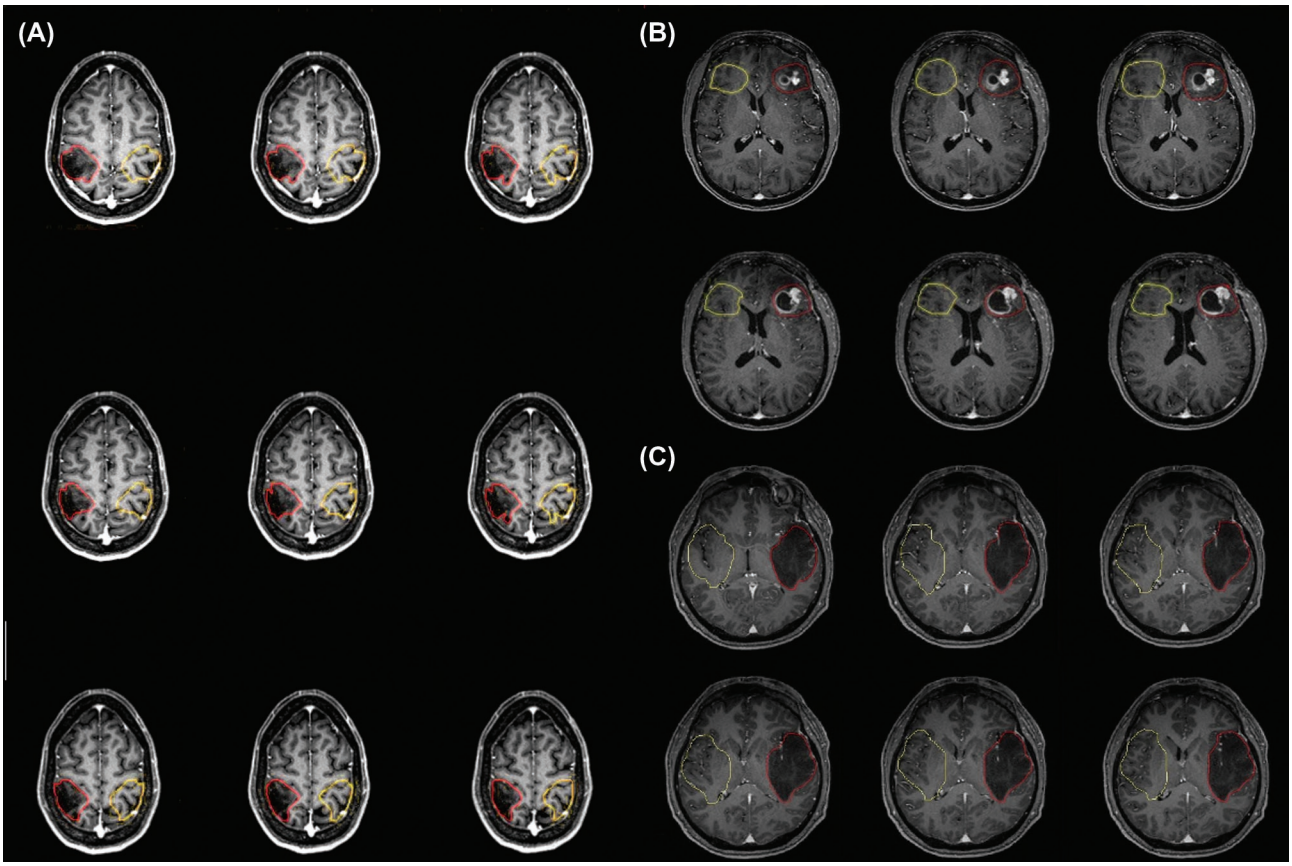

Figure 1: Examples of ROIs as drawn by one of the two observers in three cases included in this study. In (**A**) the ROI encompasses the entire lesion with most of the primary sensorimotor cortex in the precentral and postcentral gyri ("ipsilesional") and its contralateral homologous region ("contralesional") in a patient with a right perirolandic grade III anaplastic astrocytoma. (**B**) represents a patient with a glioblastoma in the left frontal lobe. In this case the lesion and part of the left inferior frontal gyrus (IFG) [Broca's area] were included in the ipsilesional ROI. Likewise the contralesional ROI included also the homologous right IFG. A patient with a grade II astrocytoma in the left temporal lobe is represented in (**C**). In this case the ipsilesional ROI encompasses the lesion and part of the expected Wernicke's area (left superior temporal gyrus) with its contralesional ROI including the right hemisphere homologue of Wernicke's area.

between grade III and IV ($z = -2.44$, $p = 0.007$ for r_{vol} and $z = -2.76$, $p = 0.003$ for r_{flow}) as well as between the group including the combination of grade II and III patients and the group including only grade IV patients ($z = -2.92$, $p = 0.002$ for r_{vol} and $z = -3.51$, $p = 0.0002$ for r_{flow}). In contrast, no statistically significant difference was found in these ratios between the grade II and grade III groups ($z = -1.30$, $p = 0.10$ for r_{vol} and $z = -0.81$, $p = 0.21$ for r_{flow}). The Kruskal Wallis tests did not report statistically significant difference in r_{CVR} distribution ($H = 4.29$, $p = 0.12$) between the different patient groups. Figure 4 shows the distribution of r_{CVR} for non hyperperfused grade II and grade III gliomas grouped together in comparison with grade IV glioblastomas characterized by angiogenesis; substantial overlap between the two groups is visible. Furthermore, the distribution of rCVR in the group was statistically significantly less than 1 in each group ($z = -1.94$, $p = 0.02$; $z = -1.89$, $p = 0.03$; $z = -2.11$, $p = 0.01$ for grade II, III and IV, respectively). In the distribution of r_{CVR} in the group including grade II and III tumors only 1 case showed a CVR ratio higher than 1 (see Figure 5). Details of the statistical analysis are reported in Table III.

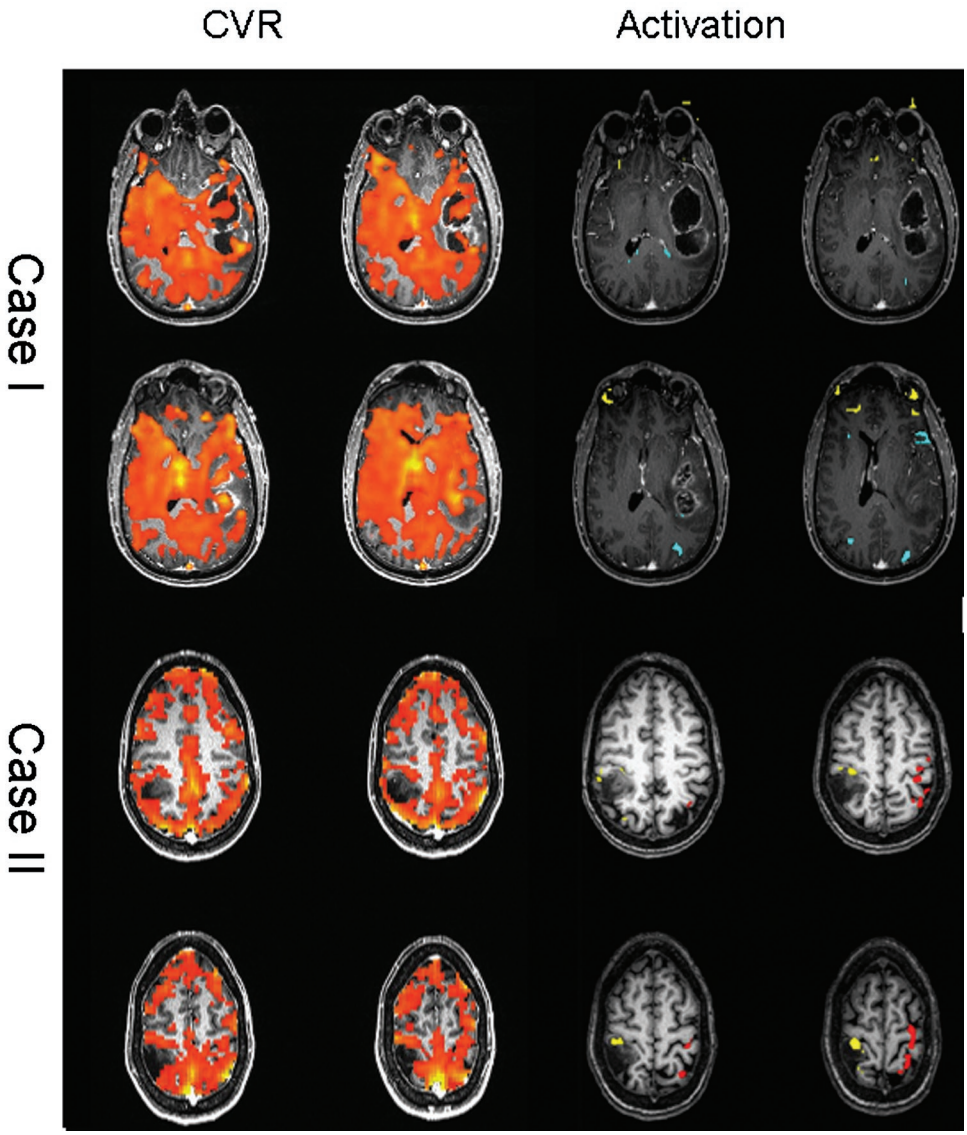

Figure 2: Example of composite BOLD activation map and corresponding CVR map for a high grade tumor (case I) and alow grade tumor (case II). In case I the composite language map, including a Silent Word Generation task (color coded cyan, 0.35 cross correlation statistical threshold) and a sentence listening comprehension task (color coded yellow, 0.35 cross correlation statistical threshold) does not show any activation corresponding to the area of decreased CVR in the left hemisphere Wernicke's area (patient is right handed). In case II a reduction of percentage signal change compared to the contralateral side in the CVR map is seen, and a composite motor activation map including a right (color coded red, 5.0 t value statistical threshold) and left (color coded yellow, 5.0 t value statistical) hand opening and closing task, shows absence of activation in the right primary somatosensory cortex corresponding to the area of regionally decreased CVR.

Table II
Patients' Functional imaging ratios for each rater.

	r_{CVR}				r_{vol}				r_{flow}			
Patient	Rater 1	Rater 2	Mean	St dev	Rater 1	Rater 2	Mean	St dev	Rater 1	Rater 2	Mean	St dev
1	−1.195	−1.000	−1.098	0.138	5.755	5.592	5.674	0.115	6.770	6.520	6.645	0.177
2	−0.270	−0.260	−0.265	0.007	3.530	3.530	3.530	0.000	4.025	4.040	4.033	0.011
3	0.010	0.012	0.011	0.001	5.160	5.588	5.374	0.303	5.390	5.700	5.545	0.219
4	0.230	0.270	0.250	0.028	2.753	2.340	2.547	0.292	3.370	2.450	2.910	0.651
5	0.290	0.270	0.280	0.014	2.184	2.920	2.552	0.520	2.280	2.950	2.615	0.474
6	0.320	0.390	0.355	0.049	2.163	2.511	2.337	0.246	3.110	3.410	3.260	0.212
7	0.416	0.460	0.438	0.031	3.908	3.922	3.915	0.010	3.940	4.700	4.320	0.537
8	0.595	0.670	0.633	0.053	3.450	3.430	3.440	0.014	3.380	3.270	3.325	0.078
9	0.766	0.873	0.819	0.075	2.873	2.799	2.836	0.053	2.882	2.807	2.845	0.052
10	0.030	0.031	0.031	0.000	2.372	2.265	2.319	0.075	2.604	2.517	2.561	0.061
11	0.560	0.563	0.562	0.002	2.541	1.609	2.075	0.659	4.764	4.343	4.554	0.298
12	0.498	0.638	0.568	0.099	2.276	2.850	2.563	0.406	2.486	3.101	2.794	0.435
13	0.427	0.573	0.500	0.104	2.722	2.467	2.594	0.180	2.771	2.583	2.677	0.133
14	0.978	1.104	1.041	0.089	3.192	3.094	3.143	0.069	3.742	3.606	3.674	0.097
15	0.042	0.094	0.068	0.037	2.273	2.141	2.207	0.093	2.282	2.256	2.269	0.018
16	0.341	0.556	0.449	0.152	1.740	1.720	1.730	0.014	1.937	1.912	1.925	0.018
17	1.231	1.558	1.395	0.232	2.654	2.518	2.586	0.096	2.766	2.755	2.761	0.008
18	0.204	0.148	0.176	0.040	2.430	2.718	2.574	0.204	2.622	2.848	2.735	0.160
19	0.446	0.381	0.414	0.046	1.404	1.314	1.359	0.064	1.494	1.392	1.443	0.072
ICC		0.972				0.943				0.947		

Discussion

Although BOLD fMRI is overall an effective presurgical mapping technique, increasing evidence suggests that the BOLD response near or within diseased cortex may be decreased and thus may not accurately reflect true neuronal activity (8, 9). In particular, the high risk of false negative activation in the vicinity of brain tumors due to NVU raises concerns about the clinical reliability of BOLD fMRI in this setting (10). Thus, the presence of lesion-induced NVU may lead to incorrect inferences regarding hemispheric lateralization and functional reorganization (11). The hypothesis investigated in this study is that BOLD BH CVR mapping will allow for better assessment of NVU risk across all grades of gliomas than T2*DSC perfusion imaging, which can only detect such risk in high grade gliomas displaying angiogenesis, in patients undergoing functional imaging for presurgical planning. To test this hypothesis, we compared CVR and perfusion metrics in a very heterogeneous sample of brain tumors, including WHO grade II, III and IV lesions.

In the grade IV group, a statistically significant (at the $p = 0.05$ level) inverse linear trend, was found between r_{CVR} and r_{flow}, in addition to a trend-level similar effect between r_{CVR} and r_{vol}. These results are intriguing because MR perfusion imaging and BH CVR mapping are fundamentally different techniques; the former represents a resting state imaging approach, while the latter represents a dynamic imaging technique that evaluates how microvasculature actively responds to a stimulus. The proliferation of neovasculature with decreased autoregulatory capacity in the cerebral cortex in the vicinity of brain tumors is the most likely explanation for these results, because the variations of BOLD MRI signal during a BH task are primarily related to changes in CBF (12). As demonstrated by Cohen *et al*., the magnitude and dynamics of the BOLD signal are heavily dependent on the basal CBF levels (13), and several clinical studies have reported uncoupling between the neural response and CBF in patients with vascular diseases (14, 15). Our results support the findings of previous studies where direct measurement of cerebrovascular reactivity was not performed.

The results for grade II and III are in agreement with a previous study that reported decreased CVR in a group of 6 grade II gliomas and 1 grade III glioma (16) and also demonstrate that possible false negatives in the BOLD activation maps due to NVU may be present also within these lesions that in general are not characterized by areas of hyperperfusion. Reduced ipsilesional CVR (r_{CVR} significantly lower than 1) and the absence of correlation between CVR and perfusion metrics suggest that T2*DSC is not capable of accurately evaluating CVR in this subset of gliomas.

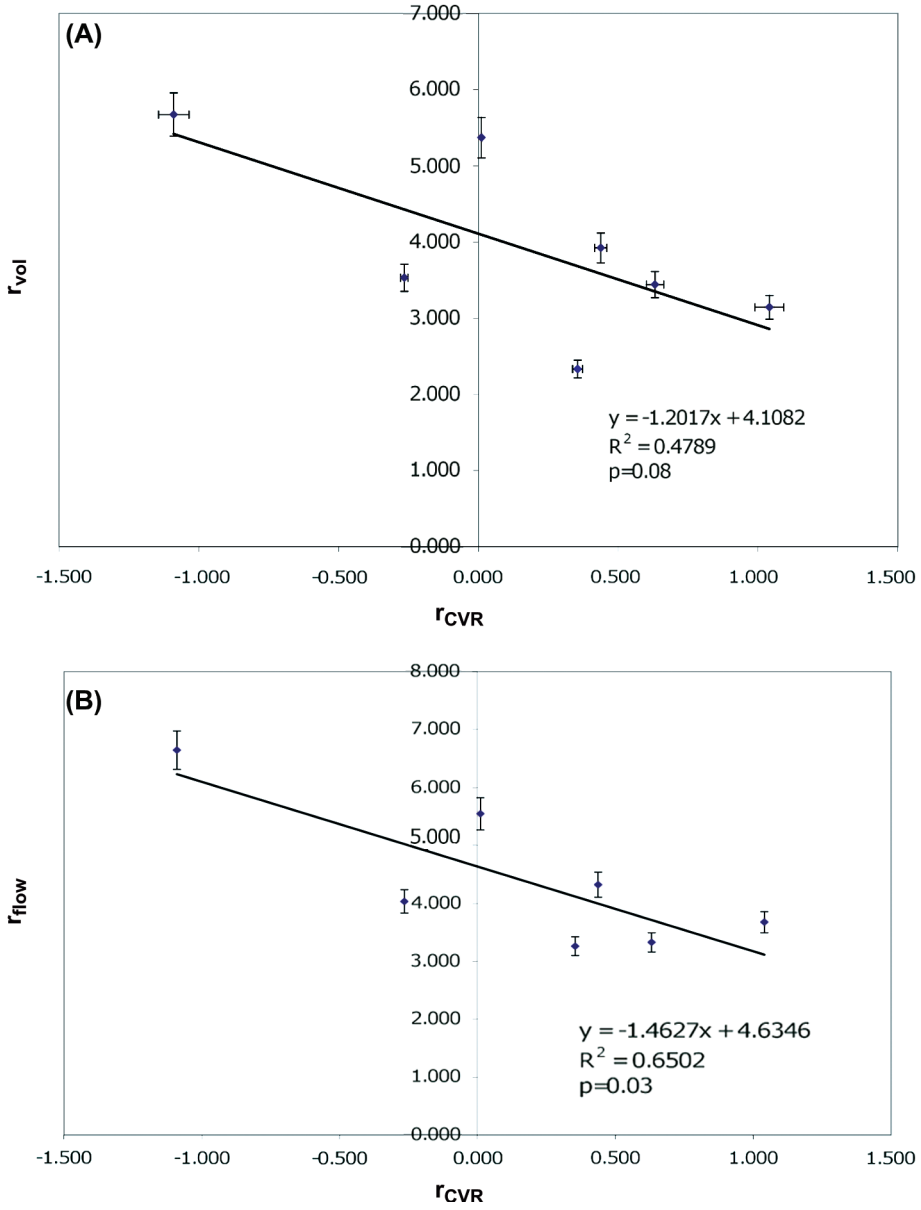

Figure 3: rCBV ratio (r_{vol}) versus CVR ratio (r_{CVR}) (**A**) and rCBF ratio (r_{flow}) versus CVR ratio (r_{CVR}) (**B**) in grade IV tumors. rCBF ratio demonstrates significant inverse correlation with CVR ratio in this grade IV tumor group.

The phenomenon of neurovascular coupling may be considered as a cascade of events, and disruption of any one of these events is sufficient to produce NVU. This neurovascular coupling cascade starts with neuronal response/electrical activity as its first component. Subsequently, synaptic transmission and associated neurotransmitters, astroctyes, chemical mediators such as nitrous oxide, prostaglandin, glutamate, Ca2+, K+, ATP, glucose and lactate, and finally the smooth muscle cells in arterioles all play important roles in the cascade (17) . Both T2*DSC perfusion imaging and BOLD BH CVR mapping only allow assessment of this final vascular component of the cascade. Dysfunction at this vascular level is a sufficient but not necessary cause of NVU, since many features of brain tumors may affect more proximal components of the cascade. In other words, impaired regional CVR implies high risk of NVU, although it cannot distinguish true negative activation from false negative activation on task-based BOLD activation maps because there may or may not be viable eloquent cortex present in a region of cortex that displays impaired CVR. However, if eloquent cortex is present at a site of regionally impaired CVR, then the presence of such impaired CVR necessarily implies the presence of NVU. However, in our sample, the presence of nearly 100% concordance between regionally decreased CVR and absent

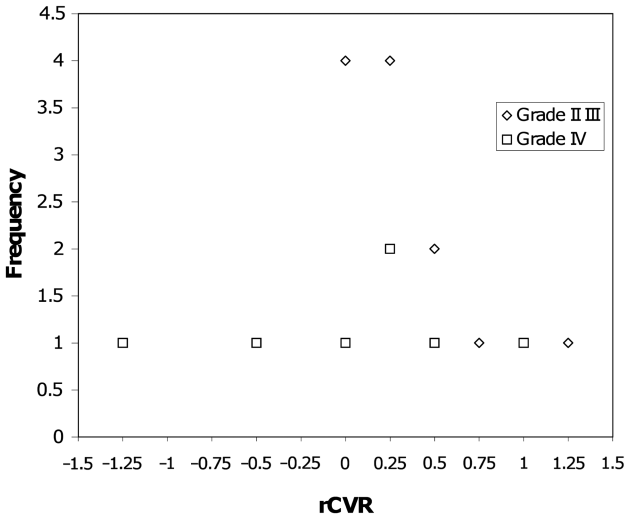

Figure 4: Histogram of the distribution of rCVR in patients with either grade II or III tumors (diamond dots) and in patients with grade IV tumors (square dots). As assessed by the Kruskall Wallis test, there is a substantial overlap between the two groups in rCVR values.

task-related BOLD activation in an area of expected eloquent cortex infiltrated by or immediately adjacent to a tumor suggests that BH CVR mapping is capable of detecting NVU. Table I demonstrates overall 94.7% concordance in our cohort of 19 patients. The one outlier represented a case in which the tumor did not actually infiltrate or abut expected eloquent cortex. Most patients referred by neurosurgeons for clinical presurgical mapping with fMRI at our institution have been selected for presurgical mapping because structural imaging demonstrates likely proximity to expected eloquent cortical regions, but this outlier case was an exception. Thus, it is not surprising that NVU was demonstrated in nearly all cases.

Whereas in high grade tumors the loss of autoregulation and CVR due to tumor angiogenesis is likely to represent the main cause for NVU (4), the infiltrative nature of glial tumors compromises also the neuronal contacts with the surrounding microvasculature and astrocytes, thus likely contributing to the attenuation of the BOLD effect even in lower grade gliomas (18, 19). However, our findings in this study are likely not related to neuronal or astrocytic dysfunction, per se, because the BH task that we employed would not be expected to result in task-correlated cortical activation, but rather would be expected to merely isolate the BOLD vascular response to a hypercapnia challenge. In addition, while in grade IV gliomas, aberrant neovascularity as manifested by abnormally increased numbers of vessels demonstrating both abnormal structure and physiology, including abnormal permeability and vasoactivity, is likely to account for the NVU, an alternative explanation may account for our similar findings of abnormally decreased CVR in lower grade gliomas. The explanation may not necessarily involve the neuronal or astrocytic/synaptic components of the neurovascular coupling spectrum, but rather may directly involve the vasculature that is infiltrated by these lower grade tumors. Specifically, the tumor infiltration at the astrocytic level may result in abnormal physiology of the relatively structurally normal vessels that permeate the lesion, which are not necessarily increased in number relative to contralateral normal brain tissue. The absence of increased vascular density within the lower grade infiltrative tumors may account for the absence of regional hyperperfusion within these lesions, but the physiologic impairment of infiltrated vasculature may result in decreased regional vasoactivity. Figures 4 and 5 demonstrate that, regardless of tumor grade, abnormally decreased ipsilesional CVR was present relative to normal homologous contralateral (*i.e.*, contralesional) regions in almost all cases; specifically, in 17 out of 19 cases, including grades II through IV, the r_{CVR} values were less than 1.0, indicative of abnormally decreased ipsilesional CVR. Only one grade IV tumor demonstrated a rCVR value of approximately 1.0, and one grade II tumor demonstrated a rCVR value slightly greater than 1.0.

The CVR maps reported for this study were obtained running a T2* BOLD EPI sequence with the patients performing a BH paradigm. This sequence represents a well-established technique for assessment of cerebrovascular reactivity because the cerebral vasculature is highly responsive to changes in blood O_2 and CO_2, and this task can be easily performed and included in a clinical functional MRI/DTI protocol for presurgical planning in brain tumor patients (20). For perfusion measurements we used a dynamic contrast-enhanced susceptibility-weighted gradient echo EPI T2* sequence because gradient echo-based rCBV measurements correlate better with tumor grade than spin echo based rCBV measurements (21). The main drawback of a gradient echo acquisition is that it is sensitive also to

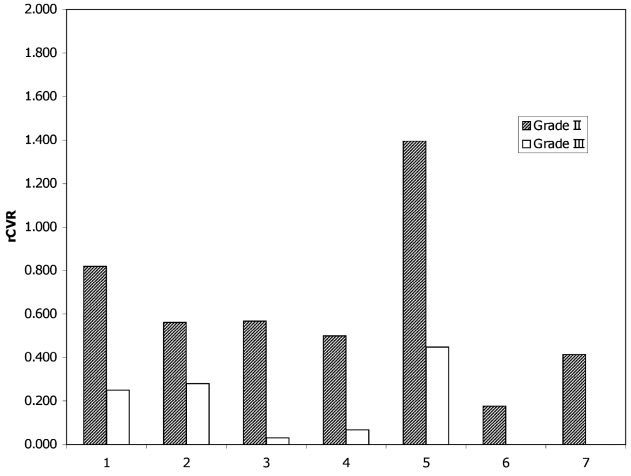

Figure 5: rCVR distribution for the group of patients with classified grade II (dashed bar) and III (white bar) tumors. In 11 out of 12 cases rCVR is less than 1. The median value is significantly less than 1 according to the One Sample Wilcoxon test.

Table III
Summary of statistical analysis results for the variables r_{CVR}, r_{vol} and r_{flow}.

	Kruskal Wallis test	One sample Wilcoxon test		
	Grade II vs. III vs. IV	Grade II	Grade III	Grade IV
r_{CVR}	$H = 4.29, p = 0.12$	$z = -1.94, p = 0.02$	$z = -1.89, p = 0.03$	$z = -2.11, p = 0.01$
		Mann Whitney test		
	Grade II vs. III	Grade II vs. IV	Grade III vs. IV	Grade II + III vs. IV
r_{vol}	$z = -1.30, p = 0.10$	$z = -2.44, p = 0.007$	$z = -2.44, p = 0.007$	$z = -2.92, p = 0.002$
r_{flow}	$z = -0.81, p = 0.21$	$z = -3.07, p = 0.001$	$z = -2.76, p = 0.003$	$z = -3.51, p = 0.0002$

macrovasculature that must be excluded from the ROI where rCBV and rCBF should be calculated. However, as stated in the Methods section, we used the postcontrast T1-weighted images to draw the ROIs where these vessels can be easily delineated and thus excluded within the ROI tracing. A post-processing algorithm was applied to correct for contrast agent extravasation because it has been demonstrated that rCBV (and rCBF) corrected for contrast leakage values correlated better with tumor grade than leakage-uncorrected perfusion metrics (7). The extravasation, indeed, causes an artificial attenuation of the first pass signal drop that in turns provides underestimation of rCBV (rCBF).

The values obtained for ICC prove that the chosen methodology provided excellent reproducibility for CVR maps as well as for rCBV and rCBF measurements as demonstrated in a previous study (22). ICC were slightly lower for rCBF (0.94) and rCBV (0.94) compared to BOLD PSC (0.97) because we chose the single pixel with the highest rCBF and rCBV within the tumor region for the perfusion metrics (r_{vol} and r_{flow}), whereas we used the mean CVR BOLD PSC in the same region. The main reason for choosing single pixels with maximal perfusion values rather than simply mean pixel values within a ROI was to avoid the risk of underestimating tumoral rCBV and rCBF. For example, in necrotic high grade gliomas, averaging of perfusion values from the highly cellular hyperperfused enhancing peripheral tumor components with the hypoperfused nonenhancing necrotic center would result in artifactually decreased mean rCBV and rCBF within the ROIs.

The choice of the ROI for tumor analysis can be controversial, especially for high grade tumors. An intuitive approach would include only the enhancing areas on the T1-weighted post contrast image. However a mismatch between the area of increased blood volume and contrast enhancement has been reported (23). For the selection of the contralateral ROI we chose the contralateral homologous normal brain tissue, including both gray and white matter (see Figure 1), whereas many previous studies reported perfusion measurements normalized to uninvolved white matter. However, either choice has been demonstrated to not have any influence on the correlation between tumor rCBV (rCBF) and tumor grade (7). Furthermore, for CVR normalization, it is important to include gray matter regions in a contralateral homologous ROI, since the pertinent changes in ipsilesional CVR have to be considered in the context of cortical signal changes rather than simply subcortical white matter CVR changes, because clinical interpretation of presurgical planning BOLD fMRI results relies solely on cortical activation.

The main limitation of this study is the relatively small sample size of the patient cohort included in this study. We presented results of 19 patients with histopathological diagnosis of WHO grade II, III or IV primary intra-axial brain tumors (*i.e.*, gliomas). The findings of this study need to be replicated on a larger scale with future studies. Another limitation of this study is related the use of a T2*DSC sequence for perfusion imaging. Despite the use of a leakage correction algorithm for more accurate rCBV estimation, contrast agent recirculation effects cannot be fully taken into account because it is a first pass based technique. Furthermore, only a relative or, at most, an approximate blood volume measurement can be obtained by this technique. The use of a T1 steady state dynamic contrast enhancement (T1 DCE) method may be considered to address some of these issues. Lastly, the BH technique does not allow any quantitative CVR measurement because it is not possible to monitor arterial pO_2 and pCO_2 levels during the task. A few medical devices have been recently developed for precise control of end-tidal pCO_2 that allow the production of quantitative maps of CVR, but their utility in a routine clinical workflow with relatively debilitated and/or poorly cooperative patients still remains problematic (24).

In conclusion, our results demonstrate that while BOLD BH CVR mapping may be similarly useful for detection of NVU risk in grade IV tumors (glioblastomas) as perfusion MR imaging, it may be uniquely suited for assessment of NVU risk in non enhancing grade II and III tumors that do not demonstrate hyperperfusion as expected in glioblastomas. Thus, this preliminary study demonstrates the feasibility

and versatility of BOLD BH CVR mapping for assessment of NVU risk across the entire spectrum of brain gliomas. The absence of aberrant tumor neovascularity (angiogenesis) and associated hyperperfusion in low grade tumors may potentially result in underestimation of NVU risk, which in turn may adversely affect the accuracy of assessments of BOLD fMRI activation maps used for presurgical mapping in these patients. Recently commercially available and accurate real time fMRI maps may help to streamline image acquisition during clinical BOLD fMRI studies, potentially obviating the need to perform CVR mapping when expected activation is seen in the language or sensorimotor cortex. However, in cases where such expected activation is not clearly seen, BH CVR mapping remains an essential element of fMRI quality control analysis, since it is able to effectively detect NVU in tumors of all grades, as demonstrated in this study.

Acknowledgement

1) The work was supported in part by a research grant from Siemens Medical Solutions (Dr. Pillai is PI), but Siemens was not involved in the study design, data collection, analysis or manuscript preparation but did provide salary support for Dr. Zaca.

2) The work was also in part supported by a research contract from the Radiological Society of North America Quantitative Imaging Biomarker Alliance (QIBA), for which Dr. Pillai is the subaward PI, and for which Dr. Daniel C. Sullivan is overall project PI [NIH NHLBI-PB-EB-2010-159-JKS "RECOVERY- Quantitative Imaging Biomarker Alliance," Subaward No.: HHSN268201000050C (19a).]

3) In addition, the DynaSuiteNeuro workstation used for part of the analysis was provided as part of a grant from Philips Healthcare to Dr. Peter van Zijl (PI, Dept. of Radiology, Johns Hopkins University), so we wish to acknowledge both Philips and Dr. van Zijl, as well as Dr. Samson Jarso for his help in setting up the DSN system.

References

1. Lehericy, S., Biondi, A., Sourour, N., Vlaicu, M., du Montcel, S.T., Cohen, L., Vivas, E., Capelle, L., Faillot, T., Casasco, A., Le Bihan, D., Marsault, C. Arteriovenous brain malformations: Is functional MR imaging reliable for studying language reorganization in patient? Initial observations. *Radiology 223*, 672-682 (2002).
2. Holodny, A. I., Schulder, M., Liu, W. C., Wolko, J., Maldjian, J. A., Kalnin, A. J. The effect of brain tumors on BOLD functional MR imaging activation in the adjacent motor cortex: Implications for image-guided neurosurgery. *AJNR Am J Neuroradiol* 21, 1415-1422 (2000).
3. Donahue, M. J., Stevens, R. D., deBoorder, M., Pekar, J. J., Hendrikse, J., van Zijl, P. C. M. Hemodynamic Changes Following Visual Stimulation and Breathholding Provide Evidence for an Uncoupling of Cerebral Blood Flow and Volume from Oxygen Metabolism. *J Cereb Blood Flow Metab 29*, 176-185 (2006).
4. Hou, B. L., Bradbury, M., Peck, K. K., Petrovich, N. M., Gutin, P. H., Holodny, A. I. Effect of brain tumor neovasculature defined by rCBV on BOLD fMRI activation volume in the primary motor cortex. *Neuroimage 32*, 489-497 (2006).
5. Kleihues, P., Burger, P. C., Scheithauer, B. W. The new WHO classification of brain tumours. *Brain Pathol 3*, 255-268 (1993).
6. Birn, R. M., Smith, M. A., Jones, T. B., Bandettini, P. A. The respiration response function: The temporal dynamics of fMRI signal fluctuations related to changes in respiration. *Neuroimage 40*, 644-654 (2008).
7. Boxerman, J. L., Schmainda, K. M., Weisskoff, R. M. Relative cerebral blood volume maps corrected for contrast agent extravasation significantly correlate with glioma tumor grade, whereas uncorrected maps do not. *AJNR Am J Neuroradiol 27*, 859-867 (2006).
8. Schreiber, A., Hubbe, U., Ziyeh, S., Hennig, J. The influence of gliomas and nonglial space-occupying lesions on blood-oxygen-level-dependent contrast enhancement. *AJNR Am J Neuroradiol 21*, 1055-1063 (2002).
9. Lee, Y. J., Chung, T. S., Young, S. Y., Lee, M. S., Han, S. H., Seong, G. J., Ahn, K. J. The role of functional MR imaging in patients with ischemia in the visual cortex. *AJNR Am J Neuroradiol 22*, 1043-1049 (2001).
10. Ulmer, J. L., Krouwer, H. G., Mueller, W. M., Ugurel, M. S., Kocak, M., Mark, L. P. Pseudo-reorganization of language cortical function at fmr imaging: A consequence of tumor-induced neurovascular uncoupling. *AJNR Am J Neuroradiol 24*, 213-217 (2003).
11. Ulmer, J. L., Hacein-Bey, L., Mathews, V. P., Mueller, W. M., DeYoe, E. A., Prost, R. W., Meyer, G. A., Krouwer, H. G., Schmainda, K. M. Lesion-induced pseudo-dominance at functional magnetic resonance imaging: Implications for preoperative assessments. *Neurosurgery 55*, 569-579 (2004).
12. Liu, H. L., Huang, J. C., Wu, C. T., Hsu, Y. Y. Detectability of blood oxygenation level-dependent signal changes during short breath hold duration. *Magn Reson Imaging 20*, 643-648 (2002).
13. Cohen, E. R., Ugurbil, K., Kim, S. G. Effect of basal conditions on the magnitude and dynamics of the blood oxygenation level-dependent fMRI response. *J Cereb Blood Flow Metab 22*, 1042-1053 (2002).
14. Jiang, Z., Krainik, A., David, O., Salon, C., Tropres, I., Hoffmann, D., Pannetier, N., Barbier, E. L., Bombin, E. R., Warnking, J., Pasteris, C., Chabardes, S., Berger, F., Grand, S., Segebarth, C., Gay, E., Le Bas, J. F. Impaired fMRI activation in patients with primary brain tumors. *Neuroimage 52*, 538-548 (2010).
15. Rossini, P. M., Altamura, C., Ferretti, A., Vernieri, F., Zappasodi, F., Caulo, M., Pizzella, V., Del Gratta, C., Romani, G. L., Tecchio, F. Does cerebrovascular disease affect the coupling between neuronal activity and local haemodynamics? *Brain 127*, 99-110 (2004).
16. Attwell, D., Buchan, A. M., Charpak, S., Lauritzen, M., MacVicar, B. A., Newman, E. A. Glial and neuronal control of brain blood flow. *Nature 468*, 232-243 (2010).
17. Paulson, O. B., Newman, E. A. Does the release of potassium from astrocyte endfeet regulate cerebral blood flow? *Science 237*, 896-898 (1987).
18. Ojemann, J. G., Miller, J. W., Silbergeld, D. L. Preserved function in brain invaded by tumor. *Neurosurgery 39*, 253-259 (1996).
19. Rostrup, E., Larsson, H. B., Toft, P. B., Garde, K., Henriksen, O. Signal changes in gradient echo images of human brain induced by hypo- and hyperoxia. *NMR Biomed 58*, 41-47 (1995).
20. Sugahara, T., Korogi, Y., Kochi, M., Ushio, Y., Takahashi, M. Perfusion-sensitive M R imaging of gliomas: Comparison between

gradient-echo and spin-echo echo-planar imaging techniques. *AJNR Am J Neuroradiol 22*, 1306-1315 (2001).
21. Wetzel, S. G., Cha, S., Johnson, G., Lee, P., Law, M., Kasow, D. L., Pierce, S. D., Xue, X. Relative cerebral blood volume measurements in intracranial mass lesions: Interobserver and intraobserver reproducibility study. *Radiology 224*, 797-803 (2002).
22. Wagner, M., Ulmer, J., Rand, S. Relationship between contrast enhancement\line and brain tumor neovascularity revealed by blood volume functional\line imaging. American Society of Neuroradiology 42nd Annual Meeting. Seattle WA, Oak Brook, II (2004).
23. Heyn, C., Poublanc, J., Crawley, A., Mandell, D., Han, J. S., Tymianski, M., terBrugge, K., Fisher, J. A., Mikulis, D. J. Quantification of cerebrovascular reactivity by blood oxygen level – Dependent MR imaging and correlation with conventional angiography in patients with moyamoya disease. *AJNR Am J Neuroradiol 31*, 862-867 (2010).

Received: September 17, 2011; Revised: December 26, 2011; Accepted: January 11, 2012